

# Perfectly Matched Layers for nonlocal Helmholtz equations Part II: higher dimensions\*

Yu Du<sup>†</sup>Jiwei Zhang<sup>‡</sup>

## Abstract

Perfectly matched layers (PMLs) are formulated and numerically applied to nonlocal Helmholtz equations in one and two dimensions. In one dimension, we give the PML modifications for the nonlocal Helmholtz equation with general kernels and show its effectiveness theoretically in some sense. In two dimensions, we give the PML modifications in both Cartesian coordinates and polar coordinates. Based on the PML modifications, nonlocal Helmholtz equations are truncated in one and two dimensional spaces, and asymptotic compatibility schemes are introduced to solve the resulting truncated problems. Finally, numerical examples are provided to study the “numerical reflections” by PMLs and verify the effectiveness and validation of our nonlocal PML strategy.

**Keywords:** nonlocal Helmholtz equation, nonlocal models, Perfectly Matched Layers, artificial boundary condition, asymptotic compatibility scheme

## 1 Introduction

In this paper, we consider solving the following nonlocal Helmholtz equation

$$\mathcal{L}u(x) - k^2u(x) = f(x), \quad x \in \mathbb{R}^d, \quad d = 1, 2, \quad (1.1)$$

by perfectly matched layers. Here  $f(x) \in L^2(\mathbb{R})$  has a bounded support  $\Omega_f$ .  $k$  is a constant related to the traditional *wavenumber* for the local Helmholtz equation and the nonlocal operator  $\mathcal{L}$  is defined by

$$\mathcal{L}u(x) = \int_{\mathbb{R}^d} (u(x) - u(y))\gamma(x, y)dy, \quad (1.2)$$

where the kernel function  $\gamma(x, y)$  satisfies

$$\gamma(x, y) \geq 0 \quad \text{and} \quad \gamma(x, y) = \gamma(y, x). \quad (1.3)$$

Note that the nonlocal Helmholtz equation shown above is defined in the whole space  $\mathbb{R}^d$ , but the far field boundary condition is not provided. The original PML technique is proposed for the standard PDEs [5] with some far field boundary conditions, such as the local Helmholtz equation

---

\*This work is supported in NSFC under grant No. 12071401, 11771035 and NSAF U1930402, Natural Science Foundation of Hunan Province No. 2019JJ50572, Natural Science Foundation of Hubei Province No. 2019CFA007 and Xiangtan University 2018ICIP01.

<sup>†</sup>Department of Mathematics, Xiangtan University, Hunan, 411105, China(duyu@xtu.edu.cn)

<sup>‡</sup>School of Mathematics and Statistics, and Hubei Key Laboratory of Computational Science, Wuhan University, Wuhan 430072, China. (jiweizhang@whu.edu.cn)

and the Maxwell's equation. A typical example is the Sommerfeld radiation condition for the local Helmholtz equation in a homogeneous medium. However, the definition of the far field boundary condition for the nonlocal Helmholtz equation is an open problem. Therefore, in this paper we simply assume that a suitable boundary condition at infinity is imposed to exclude energy incoming from infinity and only to allow energy outgoing to infinity.

While most of works are carried out for the simulation of nonlocal problems with free or fixed boundary conditions on bounded domains [13, 30, 31, 36, 25, 9, 17], there are applications where the simulation in an infinite medium might be more reasonable, such as wave or crack propagation in the whole space. We have shown that the nonlocal Helmholtz equation can be used to describe the nonlocal wave propagation in [16].

However, the unboundedness of the spatial domain presents a new computational challenge, since a naive spatial discretization generally leads to an infinite number of degrees of freedom for classical numerical methods such as finite element and finite difference methods. The objective of this paper is to develop an efficient computation of the nonlocal Helmholtz equation by constructing PMLs, an absorbing boundary condition.

Absorbing boundary conditions (ABCs) are successful approaches to simulate the wave behaviors in a physical domain of interest by imposing a suitable boundary condition, to absorb the impinging wave at artificial boundaries. The construction of tractional ABCs for local problems has been well studied [1, 20, 19, 18, 29, 21, 3], and there are also much progress for nonlocal problems [27, 34, 35, 33, 33]. PML was originally proposed by Berénger [5], which involves surrounding the computational cell with a medium that in theory absorbs without any reflection electromagnetic waves at all frequencies and angles of incidence. PML has been a popular and effective method for solving wave scattering problems [2, 8, 6, 12, 32, 23, 11, 10, 4, 24, 7, 22]. In [16] we have developed perfectly matched layers as ABCs for the one-dimensional nonlocal Helmholtz equation with kernels which are radial and satisfy some additional conditions. In this paper, we shall construct perfectly matched layers for the nonlocal Helmholtz equation in one and two dimensions. In one dimension, we develop the nonlocal PML equation in the whole space for kernels which are more general comparing with our previous work [16]. In two dimensions, we develop the nonlocal PML equation in the whole space for kernels satisfying (1.3). Particularly, we introduce two kinds of PMLs in both Cartesian coordinates and polar coordinates. The main process to derive ABCs is as follows. We first rewrite the nonlocal Helmholtz equation (1.1) as the weak form. Then we define variable changes to analytically continue to the complex plane. Finally we replace real variables in the nonlocal equation of integral form by complex variables, and get the nonlocal PML equation.

The rest of this paper is as follows. In Section 2 we derive nonlocal PML equations by extending complex coordinate transforms for the local Helmholtz equation. In Section 3, we simply show the efficiency of our PMLs theoretically in one dimension for some kernels in some sense. In Section 4 we truncate the nonlocal the computational region by putting homogeneous Dirichlet boundary conditions, and introduce AC schemes for numerically solving the truncated problems. In Section 5, numerical examples in one and two dimensions are provided to study the “numerical reflections” caused by PML modifications and verify the effectiveness of our PMLs.

## 2 Nonlocal Perfectly Matched Layers

In [16], we have given the nonlocal PMLs for the radial kernel  $\gamma(x, y) = \gamma_r(x - y)$  in one dimension, where  $\delta$  is a positive constant. In this section, we use the same key idea to derive the nonlocal PMLs

for the symmetric kernel  $\gamma(x, y)$  in one and two dimensions.

## 2.1 PML in one dimension

We use the idea for deriving the nonlocal PMLs for the radial kernel  $\gamma(x, y) = \gamma_r(x - y)$  ([16]) to get the nonlocal PMLs for general kernels in 1D.

Let  $\Omega = [-l, l]$ , ( $l > 0$ ), be a bounded domain including  $\Omega_f$ , i.e.,  $\Omega_f \subset \Omega$ , (Figure 2.1a). We define the following analytic continuation to the complex plane

$$\tilde{x} := \int_0^x \alpha(t) dt = \int_0^x \left(1 + \frac{z}{k} \sigma(t)\right) dt, \quad \tilde{y} := \int_0^y \alpha(t) dt = \int_0^y \left(1 + \frac{z}{k} \sigma(t)\right) dt. \quad (2.1)$$

Here  $\sigma(t) = 0$  in  $\Omega$ , and is positive inside the PMLs, i.e.,  $\sigma(t) > 0$  in  $\mathbb{R} \setminus \Omega$ .  $z$  is a complex parameter, such as  $i$  or  $1 + i$ . This mapping has the effect of transforming traveling waves of the form  $e^{ikx}$  into evanescent waves of the form  $e^{ik\Re\tilde{x}} e^{-k\Im\tilde{x}}$  when the imaginary part of  $z$  is positive.

We have the weak form of Eq. (1.1)

$$(\mathcal{L}u, v) - k^2(u, v) = (f, v), \quad \forall v \in C_0^\infty(\mathbb{R}), \quad (2.2)$$

where  $(\cdot, \cdot)$  denotes the inner product in the complex valued  $L^2$ -space. We have

$$(\mathcal{L}u, v) = \frac{1}{2} \int_{\mathbb{R}} \int_{\mathbb{R}} (u(x) - u(y)) (\bar{v}(x) - \bar{v}(y)) \gamma(x, y) dy dx, \quad (2.3)$$

where  $\bar{v}(x)$  represents the complex conjugate of  $v(x)$ .

By replacing

$$x \rightarrow \tilde{x}, \quad y \rightarrow \tilde{y}, \quad \text{and} \quad dx \rightarrow \frac{\partial \tilde{x}}{\partial x} dx = \alpha(x) dx, \quad dy \rightarrow \frac{\partial \tilde{y}}{\partial y} dy = \alpha(y) dy,$$

we get the following nonlocal equation with PML modifications

$$\begin{aligned} \frac{1}{2} \int_{\mathbb{R}} \int_{\mathbb{R}} (\tilde{u}(x) - \tilde{u}(y)) (\tilde{v}(x) - \tilde{v}(y)) \gamma(\tilde{x}, \tilde{y}) \alpha(x) \alpha(y) dy dx \\ - k^2 \int_{\mathbb{R}} \tilde{u}(x) \tilde{v}(x) \alpha(x) dx = \int_{\mathbb{R}} f(x) \tilde{v}(x) \alpha(x) dx, \end{aligned} \quad (2.4)$$

where  $\tilde{u}(x) := u(\tilde{x})$ ,  $\tilde{u}(y) := u(\tilde{y})$ ,  $\tilde{v}(x) := \bar{v}(\tilde{x})$  and  $\tilde{v}(y) := \bar{v}(\tilde{y})$ . Using the facts  $\alpha(x) = 1$ ,  $\tilde{x} = x$ ,  $\forall x \in \Omega$  and  $\text{supp} f(x) \subset \Omega$ , we have the strong form of (2.4)

$$\tilde{\mathcal{L}}\tilde{u}(x) - k^2\alpha(x)\tilde{u}(x) = f(x), \quad (2.5)$$

where the nonlocal operator with PML modifications is given by

$$\tilde{\mathcal{L}}\tilde{u}(x) = \int_{\mathbb{R}} (\tilde{u}(x) - \tilde{u}(y)) \gamma(\tilde{x}, \tilde{y}) \alpha(x) \alpha(y) dy. \quad (2.6)$$

## 2.2 PMLs in two dimensions

Here let's go to the nonlocal PMLs for the nonlocal equation in two dimensions.

Let  $\Omega$  be a bounded domain including  $\Omega_f$ , such as  $\Omega = [-l, l]^2$  and  $\Omega = \{(x, y) : \sqrt{x^2 + y^2} \leq l_r\}$ , (Figures 2.1b and 2.1c).

Denote by  $\tilde{x} = (\tilde{x}_1(x), \tilde{x}_2(x))$  and  $\tilde{y} = (\tilde{y}_1(y), \tilde{y}_2(y))$  the variable changes of  $x = (x_1, x_2)$  and  $y = (y_1, y_2)$ , respectively, which satisfy  $\tilde{x} = x$ ,  $\tilde{y} = y \forall x, y \in \Omega$  and are complex in the PMLs  $\mathbb{R}^2 \setminus \Omega$ .

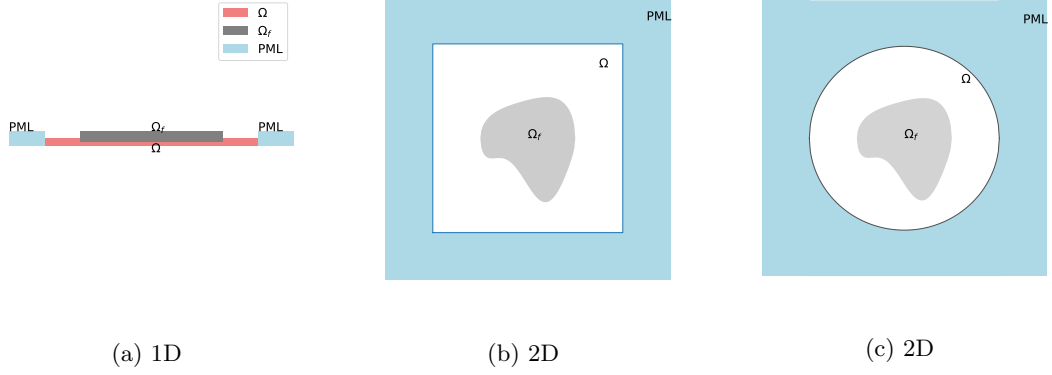


Figure 2.1:  $\Omega_f$ ,  $\Omega$  and the PML “absorbing” regions. In the “absorbing” regions, the PML absorption coefficients  $\sigma$  (1D),  $\sigma_j, j = 1, 2$  (in Cartesian coordinates in 2D) and  $\sigma_r$  (in polar coordinates in 2D) are positive, respectively. In  $\Omega$ , these PML absorption coefficients are zero.

We consider two kinds of variable changes in this paper, one is in Cartesian coordinates and the other in polar coordinates.

We also consider the weak form of Eq. (1.1) in two dimensions

$$\frac{1}{2} \int_{\mathbb{R}^2} \int_{\mathbb{R}^2} [u(x) - u(y)] [\bar{v}(x) - \bar{v}(y)] \gamma(x, y) dy dx - k^2 \int_{\mathbb{R}^2} u(x) \bar{v}(x) dx = \int_{\mathbb{R}^2} f(x) \bar{v}(x) dx. \quad (2.7)$$

By replacing

$$x \rightarrow \tilde{x}, y \rightarrow \tilde{y}, dx \rightarrow \frac{\partial \tilde{x}}{\partial x} dx = \begin{vmatrix} \frac{\partial \tilde{x}_1}{\partial x_1} & \frac{\partial \tilde{x}_2}{\partial x_1} \\ \frac{\partial \tilde{x}_1}{\partial x_2} & \frac{\partial \tilde{x}_2}{\partial x_2} \end{vmatrix} dx, dy \rightarrow \frac{\partial \tilde{y}}{\partial y} dy = \begin{vmatrix} \frac{\partial \tilde{y}_1}{\partial y_1} & \frac{\partial \tilde{y}_2}{\partial y_1} \\ \frac{\partial \tilde{y}_1}{\partial y_2} & \frac{\partial \tilde{y}_2}{\partial y_2} \end{vmatrix} dy,$$

we get the nonlocal PML equation of integral form

$$\begin{aligned} \frac{1}{2} \int_{\mathbb{R}^2} \int_{\mathbb{R}^2} [u(\tilde{x}) - u(\tilde{y})] [\bar{v}(\tilde{x}) - \bar{v}(\tilde{y})] \gamma(\tilde{x}, \tilde{y}) \frac{\partial \tilde{x}}{\partial x} \frac{\partial \tilde{y}}{\partial y} dy dx \\ - \int_{\mathbb{R}^2} k^2 u(\tilde{x}) \bar{v}(\tilde{x}) \frac{\partial \tilde{x}}{\partial x} dx = \int_{\mathbb{R}^2} f(\tilde{x}) \bar{v}(\tilde{x}) \frac{\partial \tilde{x}}{\partial x} dx. \end{aligned} \quad (2.8)$$

The corresponding strong form of the nonlocal PML equation is given by

$$\tilde{\mathcal{L}}\tilde{u}(x) - k^2 \frac{\partial \tilde{x}}{\partial x} \tilde{u}(x) = f(x), \quad (2.9)$$

where

$$\tilde{\mathcal{L}}\tilde{u}(x) = \int_{\mathbb{R}^2} [\tilde{u}(x) - \tilde{u}(y)] \gamma(\tilde{x}, \tilde{y}) \frac{\partial \tilde{x}}{\partial x} \frac{\partial \tilde{y}}{\partial y} dy. \quad (2.10)$$

Note that the right hand side is still  $f(x)$  since  $\tilde{x} = x$  in  $\Omega$  and  $\text{supp} f \subset \Omega$ .

Next we introduce two kinds of PMLs in Cartesian coordinates and polar coordinates, respectively.

### 2.2.1 PML in Cartesian coordinates

We first introduce the PMLs obtained by stretching Cartesian coordinates. For simplicity, we choose  $\Omega$  as a square centered at  $(0, 0)$ , i.e.,  $\Omega = [-l, l]^2$ , where  $l$  is chosen such that  $\Omega_f \subset \Omega$ . The change of variables is given by

$$\tilde{x} = (\tilde{x}_1(x_1), \tilde{x}_2(x_2)), \quad \tilde{y} = (\tilde{y}_1(y_1), \tilde{y}_2(y_2)),$$

where

$$\tilde{x}_j(x_j) = \int_0^{x_j} \alpha_j(t) dt = x_j + \frac{z_j}{k} \int_0^{x_j} \sigma_j(t) dt, \quad (2.11)$$

$$\tilde{y}_j(y_j) = \int_0^{y_j} \alpha_j(t) dt = y_j + \frac{z_j}{k} \int_0^{y_j} \sigma_j(t) dt. \quad (2.12)$$

$\sigma_j(t) = 0 (j = 1, 2)$  in  $[-l, l]$  and are positive in  $(-\infty, -l) \cup (l, +\infty)$ .  $z_j (j = 1, 2)$  are complex parameters, such as  $i$  and  $1+i$ .

By simple calculations we get

$$\begin{pmatrix} \frac{\partial \tilde{x}_1}{\partial x_1} & \frac{\partial \tilde{x}_2}{\partial x_1} \\ \frac{\partial \tilde{x}_1}{\partial x_2} & \frac{\partial \tilde{x}_2}{\partial x_2} \end{pmatrix} = \begin{pmatrix} \alpha_1(x_1) & 0 \\ 0 & \alpha_2(x_2) \end{pmatrix} \implies \frac{\partial \tilde{x}}{\partial x} = \alpha_1(x_1)\alpha_2(x_2), \quad (2.13)$$

$$\begin{pmatrix} \frac{\partial \tilde{y}_1}{\partial y_1} & \frac{\partial \tilde{y}_2}{\partial y_1} \\ \frac{\partial \tilde{y}_1}{\partial y_2} & \frac{\partial \tilde{y}_2}{\partial y_2} \end{pmatrix} = \begin{pmatrix} \alpha_1(y_1) & 0 \\ 0 & \alpha_2(y_2) \end{pmatrix} \implies \frac{\partial \tilde{y}}{\partial y} = \alpha_1(y_1)\alpha_2(y_2). \quad (2.14)$$

Therefore, by (2.9)–(2.10) the nonlocal PML equation is given by

$$\int_{\mathbb{R}^2} [\tilde{u}(x) - \tilde{u}(y)] \gamma(\tilde{x}, \tilde{y}) \alpha_1(x_1)\alpha_2(x_2)\alpha_1(y_1)\alpha_2(y_2) dy - k^2 \alpha_1(x_1)\alpha_2(x_2)\tilde{u}(x) = f(x).$$

## 2.2.2 PML in polar coordinates

Here we derive the nonlocal PMLs by stretching the radial coordinate. In this case, for simplicity we choose  $\Omega = \{(x, y) : \sqrt{x^2 + y^2} \leq l_r\}$  where  $l_r$  is a constant such that  $\Omega_f \subset \Omega$ , (Figure 2.1c). Denote by  $(r_x, \theta_x)$  and  $(r_y, \theta_y)$  the polar coordinates of  $x, y \in \mathbb{R}^2$ , respectively. We define the change of variables  $r_x$  and  $r_y$

$$\tilde{r}_x = \int_0^{r_x} \alpha_r(t) dt = r_x + \frac{z}{k} \int_0^{r_x} \sigma_r(t) dt, \quad (2.15)$$

$$\tilde{r}_y = \int_0^{r_y} \alpha_r(t) dt = r_y + \frac{z}{k} \int_0^{r_y} \sigma_r(t) dt. \quad (2.16)$$

$\sigma_r(t) = 0$  in  $[0, l_r]$  and is positive in  $(l_r, +\infty)$ .  $z$  is a complex parameter. Then in this case the complex coordinate stretching is given by

$$x_1 \rightarrow \tilde{x}_1(x) = \tilde{r}_x \cos \theta_x, \quad x_2 \rightarrow \tilde{x}_2(x) = \tilde{r}_x \sin \theta_x, \quad (2.17)$$

$$y_1 \rightarrow \tilde{y}_1(y) = \tilde{r}_y \cos \theta_y, \quad y_2 \rightarrow \tilde{y}_2(y) = \tilde{r}_y \sin \theta_y. \quad (2.18)$$

By calculations we obtain

$$\begin{pmatrix} \frac{\partial \tilde{x}_1}{\partial x_1} & \frac{\partial \tilde{x}_2}{\partial x_1} \\ \frac{\partial \tilde{x}_1}{\partial x_2} & \frac{\partial \tilde{x}_2}{\partial x_2} \end{pmatrix} = \begin{pmatrix} \cos \theta_x & -\sin \theta_x \\ \sin \theta_x & \cos \theta_x \end{pmatrix} \begin{pmatrix} \alpha_r(r_x) & 0 \\ 0 & \beta(r_x) \end{pmatrix} \begin{pmatrix} \cos \theta_x & \sin \theta_x \\ -\sin \theta_x & \cos \theta_x \end{pmatrix}, \quad (2.19)$$

where  $\beta(r_x) = \tilde{r}_x/r_x$ , which implies

$$\frac{\partial \tilde{x}}{\partial x} = \alpha_r(r_x)\beta(r_x). \quad (2.20)$$

Similarly, we have

$$\frac{\partial \tilde{y}}{\partial y} = \alpha_r(r_y)\beta(r_y). \quad (2.21)$$

By (2.9)–(2.10), we get the nonlocal PML equation

$$\int_{\mathbb{R}^2} [\tilde{u}(x) - \tilde{u}(y)] \gamma(\tilde{x}, \tilde{y}) \alpha_r(r_x)\beta(r_x)\alpha_r(r_y)\beta(r_y) dy - k^2 \alpha_r(r_x)\beta(r_x)\tilde{u}(x) = f(x). \quad (2.22)$$

**Remark 2.1** We provide PMLs in one and two dimensions here and the reader can use the same idea to derive PMLs in higher dimensions.

### 3 Efficiency of the PML technique in one dimension

In this section we show the efficiency of the PML technique for radial kernels in one dimension in some sense.

We assume that the kernel  $\gamma(x, y)$ ,  $(x, y \in \mathbb{R})$ , is radial, i.e.,  $\gamma(x, y) = \gamma_r(x - y)$ , where  $\gamma_r(x - y)$  satisfies the following conditions [16]:

- nonnegativeness:  $\gamma_r(s) \geq 0$ ;
- symmetry in  $s$ :  $\gamma_r(s) = \gamma_r(-s)$ ;
- finite horizon:  $\gamma_r(s) = 0$  for  $|s| > \delta$ ;
- the second moment condition:  $\frac{1}{2} \int_{\mathbb{R}} s^2 \gamma_r(s) ds = 1$ .

We still denote by  $u(x)$  the solution to Eq. (1.1) with the kernel  $\gamma_r(x - y)$ . We introduce the following function which play a key role in the proof,

$$G_{x_0}(x) = \begin{cases} C_1(x_0)e^{-i\tilde{k}x}, & x \leq x_0 \quad \text{with} \quad C_1(x_0) = -\frac{e^{i\tilde{k}x_0}}{2i\tilde{k}}, \\ C_2(x_0)e^{i\tilde{k}x}, & x > x_0 \quad \text{with} \quad C_2(x_0) = -\frac{e^{-i\tilde{k}x_0}}{2i\tilde{k}}, \end{cases} \quad (3.1)$$

where  $\tilde{k}$ , which is a positive real number or a complex with positive imaginary part, is the solution of

$$\int_{\mathbb{R}} (1 - e^{i\tilde{k}s}) \gamma_r(s) ds = k^2. \quad (3.2)$$

We define an average of  $u$

$$u^a(x) := \int_{\mathbb{R}} u(t + x) \kappa(t) dt, \quad (3.3)$$

where the weight  $\kappa(t)$  is an even function and is equal to

$$\kappa(t) = -\frac{1}{k} \int_t^{+\infty} \sin \tilde{k}(t - s) \gamma_r(s) ds, \quad \text{for } t > 0. \quad (3.4)$$

Particularly, we denote by  $u^e$  the solution to (1.1) with the kernel  $\gamma_r(x - y) = \frac{1}{2c_\gamma^3} e^{-\frac{|x-y|}{c_\gamma}}$  where  $c_\gamma$  is a positive constant.

From [16], we know that the average  $u^a$  and the particular solution  $e^e$  are given by

$$u^a(x) = \int_{\mathbb{R}} G_x(y) f(y) dy. \quad (3.5)$$

and

$$u^e(x) = \int_{\mathbb{R}} \left( \frac{1}{(1 - (c_\gamma k)^2)^2} G_x(y) + \frac{c_\gamma^2}{1 - (c_\gamma k)^2} \mathcal{D}(y - x) \right) f(y) dy, \quad (3.6)$$

where  $\mathcal{D}(x - x_0)$  is used to represent the Dirac delta function. In Eq. (3.6), we can get  $\tilde{k} = k\sqrt{1/(1 - (c_\gamma k)^2)}$  by Eq. (3.2).

Note that Eq. (3.6) actually gives the Green's function of the nonlocal Helmholtz equation with the kernel  $\gamma_r(x-y) = \frac{1}{2c_\gamma^2} e^{-\frac{|x-y|}{c_\gamma}}$ , i.e.,

$$G_x^e(y) = \frac{1}{(1-(c_\gamma k)^2)^2} G_x(y) + \frac{c_\gamma^2}{1-(c_\gamma k)^2} \mathcal{D}(y-x).$$

This Green's function has the asymptotic property with the Green's function of the local Helmholtz equation with Sommerfeld radiation boundary condition [26], that is, converges to the local Green's function when  $c_\gamma \rightarrow 0$ .

We have the following results showing that the PML is an efficient technique in one dimension for some  $z$ .

**Theorem 3.1** *Assume that  $\Omega = [-l, l]$  and denote by  $\chi(x) = |\int_0^x \sigma(t) dt|$ . Let  $z = z^r + iz^i$  ( $z^r \geq 0, z^i > 0$ ). When  $\frac{z^r}{z^i}$  is large enough,  $u^a(x)$  and  $u^e(x)$  with PML modifications, i.e.,  $u^a(\tilde{x})$  and  $u^e(\tilde{x})$ , decay exponentially as  $|x| \rightarrow \infty$ :*

1 if  $\tilde{k} \in \mathbb{R}$  is positive, for any  $z^r \geq 0, z^i > 0$ ,

$$|u^a(\tilde{x})| \leq \frac{\sqrt{l}}{\sqrt{2\tilde{k}}} e^{-\frac{\tilde{k}}{k} z^i |x|} \|f\|_{L^2(\Omega)}, \quad \text{for } |x| > l, \quad (3.7)$$

$$|u^e(\tilde{x})| \leq \frac{\sqrt{l}}{\sqrt{2\tilde{k}}(1-(\delta k)^2)^2} e^{-\frac{\tilde{k}}{k} z^i |x|} \|f\|_{L^2(\Omega)}, \quad \text{for } |x| > l; \quad (3.8)$$

2 if  $\tilde{k}$  is a complex constant with positive imaginary part, i.e.,  $\Im(\tilde{k}) > 0$ , for any  $\lambda \in (0, 1)$ , when  $\frac{z^r}{z^i} \geq -\frac{1}{1-\lambda} \frac{\Re(\tilde{k})}{\Im(\tilde{k})}$ ,

$$|u^a(\tilde{x})| \leq \frac{\sqrt{l}}{\sqrt{2|\tilde{k}|}} e^{-\lambda \Im(\tilde{k})(|x + \frac{z^r}{k} \chi| - l)} \|f\|_{L^2(\Omega)}, \quad \text{for } |x| > l, \quad (3.9)$$

$$|u^e(\tilde{x})| \leq \frac{\sqrt{l}}{\sqrt{2|\tilde{k}|}(1-(\delta k)^2)^2} e^{-\lambda \Im(\tilde{k})(|x + \frac{z^r}{k} \chi| - l)} \|f\|_{L^2(\Omega)}, \quad \text{for } |x| > l. \quad (3.10)$$

*Proof.* Inequalities (3.7) and (3.8) can be obtained by the same arguments in [16, Theorem 1], and we omit the details.

Next we prove (3.9). For  $x > l$ ,

$$\begin{aligned} |u^a(\tilde{x})| &= \left| \int_{\Omega} G_{\tilde{x}}(y) f(y) dy \right| = \left| \int_{\Omega} C_0 e^{i\tilde{k}((\Re(\tilde{x})-y) + i\Im(\tilde{x}))} f(y) dy \right| \\ &\leq \frac{1}{2|\tilde{k}|} \left( \int_{\Omega} e^{-2(\Im(\tilde{k})(\Re(\tilde{x})-y) + \Re(\tilde{k})\Im(\tilde{x}))} dy \right)^{\frac{1}{2}} \|f\|_{L^2(\Omega)} \\ &\leq \frac{\sqrt{2l}}{2|\tilde{k}|} e^{-(\Im(\tilde{k})(\Re(\tilde{x})-l) + \Re(\tilde{k})\Im(\tilde{x}))} \|f\|_{L^2(\Omega)}. \end{aligned} \quad (3.11)$$

Note that  $\Re(\tilde{x}) = x + \frac{z^r}{k} \chi$ ,  $\Im(\tilde{x}) = \frac{z^r}{k} \chi$  and  $\chi(x) > 0$  when  $x > l$ . By simple calculations, we have when  $\frac{x-l}{\chi} \frac{k}{z^i} + \frac{z^r}{z^i} \geq -\frac{1}{1-\lambda} \frac{\Re(\tilde{k})}{\Im(\tilde{k})}$ ,

$$\Im(\tilde{k})(\Re(\tilde{x}) - l) + \Re(\tilde{k})\Im(\tilde{x}) = \Im(\tilde{k})(x + \frac{z^r}{k} \chi - l) + \Re(\tilde{k}) \frac{z^r}{k} \chi \geq \lambda \Im(\tilde{k})(x + \frac{z^r}{k} \chi - l). \quad (3.12)$$

Combining (3.11) and (3.12), we get (3.9) for  $x > l$ . We can also get (3.9) for  $x < -l$  by similar arguments.

Finally, we derive (3.10) in analogy to (3.11)–(3.12).

**Remark 3.1** In [16], it's shown that for complex  $\tilde{k}$  with positive imaginary part,  $u^a(x)$  and  $u^e(x)$  themselves decay exponentially as  $|x| \rightarrow \infty$ . In this case one might object that an evanescent wave is decaying anyway, so we hardly need a PML—we just need to make the computational region large enough and it will go away on its own. This is true, but it is hard to judge whether  $\tilde{k}$  is real or complex by Eq. (3.2) for many kernels and it would be nice to accelerate the process: in some cases  $\Im(\tilde{k})$  may be relatively small and would need a large grid for it to decay sufficiently. We can easily make  $z^r \chi$  large to accelerate the decay of evanescent waves without creating any reflections.

Adding a large  $z^r$  does come at a price, however. What it does to the propagating (real  $\tilde{k}$ ) waves is to make them oscillate faster and possibly exacerbates the numerical reflections, which can be observed in our numerical tests (Examples 1.3 and 1.4 in Section 5). In short, everything in moderation.

## 4 Numerically solving the PML equations

In this section, we solve nonlocal PML equations by truncating the computational region and finite difference methods of integral form.

### 4.1 Truncating computational regions

Note that nonlocal Helmholtz equations with PML modifications is still on unbounded domain, thus we need to truncate computational regions. Once we have performed the PML transformation of our wave equations, solutions are unchanged in our region of interest  $\Omega$  and exponentially decaying in the outer regions  $\mathbb{R}^d \setminus \Omega$ . That means that we can truncate the computational region at some sufficiently large  $x$  by putting a hard wall, (Dirichlet boundary condition).

Denote by  $\Omega_p$  PML layers, such as

$$\Omega_p = \Omega_p^s := \{x \in \mathbb{R}^d \setminus \Omega \mid \inf_{y \in \Omega} |x - y|_\infty < d_{pml}\}, \quad (\text{Figures 4.1a and 4.1b}), \quad (4.1)$$

and

$$\Omega_p = \Omega_p^c := \{x \in \mathbb{R}^d \setminus \Omega \mid \inf_{y \in \Omega} |x - y|_2 < d_{pml}\}, \quad (\text{Figure 4.1c}) \quad (4.2)$$

where  $d_{pml}$  is some positive constant and is denoted by the width of PML layers.

Denote by  $\Omega_b$  the boundary layer

$$\Omega_b := \{x \in \mathbb{R}^d \setminus (\Omega \cup \Omega_p) \mid \text{dist}(x, \Omega_p) \leq \delta\}.$$

Note that the definition of  $\text{dist}(x, \Omega_p)$  depends on the kernel  $\gamma(x, y)$ . For example, if  $\gamma(x, y) = 0$  when  $|x - y|_\infty > \delta$ , we have  $\text{dist}(x, \Omega_p) := \inf_{y \in \Omega_p} |x - y|_\infty$  (Figure 4.1b), and if  $\gamma(x, y) = 0$  when  $|x - y|_2 > \delta$ , we have  $\text{dist}(x, \Omega_p) := \inf_{y \in \Omega_p} |x - y|_2$  (Figure 4.1c). For more discussions on nonlocal constraints defined on a domain with a nonzero volume we refer to [28, 30, 14, 9], etc.

We get the following truncated nonlocal PML equation subject to a nonlocal constraint of the Dirichlet type

$$\tilde{\mathcal{L}}\hat{u}(x) - k^2 \frac{\partial \tilde{x}}{\partial x} \hat{u}(x) = f(x), \quad x \in \Omega \cup \Omega_p, \quad (4.3)$$

$$\hat{u}(x) = 0, \quad x \in \Omega_b. \quad (4.4)$$

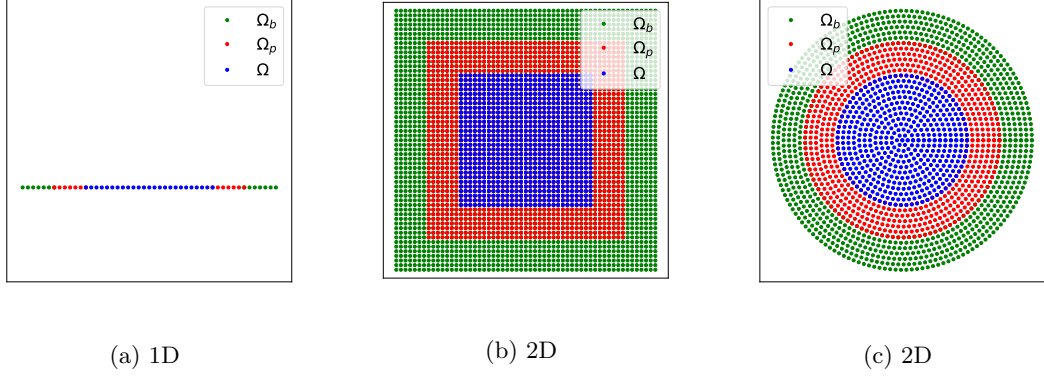


Figure 4.1: Truncated domains in one and two dimensions. Left: 1D. Middle:  $\Omega$  is a square and  $\Omega_p = \Omega_p^s$  in 2D. Right:  $\Omega$  is a circle and  $\Omega_p = \Omega_p^c$  in 2D.

**Remark 4.1** (a) *Because only the tiny exponential tails “see” this hard wall and reflect off it, and even they attenuate on the way back towards the region of interest, the effect on the solutions in our region of interest will be exponentially small.*

(b) *In principle we can make the PML region as thin as we want, just by making the real part or imaginary part of  $z$  very large (which make the exponentially decay rate rapid under the assumption that  $\sigma$  (or  $\sigma_j$ ,  $\sigma_r$  in 2D) is less than or equal to 1 over  $\Omega$ ). However, in practice, we will see in Section 5 that using a very large  $z$  can cause “numerical reflections” once we discretize the problem on a grid.*

## 4.2 The discretization scheme

We now use an AC quadrature-based finite difference discretization to solve truncated PML equations. The method was proposed by Du et al. [15]. to solve multidimensional nonlocal diffusion and wave propagation models, and we extend it to solving the nonlocal PML equations (4.3)–(4.4).

### 4.2.1 One dimension

Let  $[-l - d_{pml} - \delta, l + d_{pml} + \delta]$  be discretized by a uniform grid  $x_{-N}, x_{-N+1}, \dots, x_N$  with spacing  $h$ . For simplicity, assume that there exist integers  $M_1$  and  $M_2$  such that  $l = M_1 h$  and  $d_{pml} = M_2 h$ . Denote by  $\tilde{\gamma}(x, y) = \gamma(\tilde{x}, \tilde{y})\alpha(x)\alpha(y)$  which is still symmetric, and by

$$\tilde{F}(x, y, s) := \frac{\hat{u}(x) - \hat{u}(y)}{y - x} s^{\tilde{\gamma}} \left( \frac{x + y}{2} - \frac{s}{2}, \frac{x + y}{2} + \frac{s}{2} \right).$$

It’s clear that

$$\tilde{\mathcal{L}}\hat{u}(x) := \int_{\mathbb{R}} \tilde{F}(x, y, y - x) dy.$$

Then we expand  $\tilde{F}(x, y, s)$  in test functions with respect to  $y$

$$\tilde{F}_h(x, y, s) = \sum_m \phi_m(y) \tilde{F}(x, x_m, s),$$

where  $\phi_m(y)$  is the hat function of width  $h$  centered at  $y_m = mh$ . The discrete formulation of  $\tilde{\mathcal{L}}$  is given by

$$\begin{aligned}\tilde{\mathcal{L}}_h \hat{u}(x_n) &= \int_{\mathbb{R}} \tilde{F}_h(x_n, y, y - x_n) dy \\ &= \int_{\mathbb{R}} \sum_m \phi_m(y) \tilde{F}(x_n, x_m, y - x_n) dy \\ &= \sum_{m \neq n} \int_{\mathbb{R}} \phi_m(y) \frac{\hat{u}(x_n) - \hat{u}(x_m)}{x_m - x_n} (y - x_n) \tilde{\gamma} \left( \frac{x_n + x_m}{2} - \frac{y - x_n}{2}, \frac{x_n + x_m}{2} + \frac{y - x_n}{2} \right) dy \\ &= \sum_{m \in \mathbb{Z}} \tilde{a}_{n,m} \hat{u}(x_m),\end{aligned}$$

where

$$\tilde{a}_{n,m} = \begin{cases} -\frac{1}{(m-n)h} \int_{\mathbb{R}} \left[ \phi_m(y) (y - x_n) \tilde{\gamma} \left( \frac{x_m + y}{2}, x_n + \frac{x_m - y}{2} \right) \right] dy, & m \neq n, \\ -\sum_{m \neq n} \tilde{a}_{n,m} & m = n. \end{cases}$$

Denote by  $\mathcal{N}$  the set of all nodes in  $\Omega$ , by  $\mathcal{N}_p$  the set of nodes in the PML region  $\Omega_p$  and by  $\mathcal{N}_b$  the set of nodes in the boundary layer  $\Omega_b$  (Figure 4.1a). The resulting quadrature-based finite difference scheme for solving the nonlocal diffusion problem can be more conveniently written as the following: find  $\{\hat{u}_h(x_n)\}$  such that

$$\begin{aligned}\tilde{\mathcal{L}}_h \hat{u}_h(x_n) - k^2 \alpha(x_n) \hat{u}_h(x_n) &= f(x_n), & x_n \in \mathcal{N} \cup \mathcal{N}_p, \\ \hat{u}_h(x_n) &= 0, & x_n \in \mathcal{N}_b.\end{aligned}$$

#### 4.2.2 Two dimensions

Let  $\{x_{\mathbf{n}} \in \Omega \cup \Omega_p \cup \Omega_b\}$  be the set of nodes of a uniform Cartesian mesh with mesh size  $h$ . Here,  $\mathbf{n} = (n_1, n_2)$  denotes a multiindex corresponding to  $x_{\mathbf{n}} = h\mathbf{n}$ . An illustration of the mesh is given by Figure 5.7 in the following numerical tests for two kinds of PMLs

Denote by  $\tilde{\gamma}(x, y) = \gamma(\tilde{x}, \tilde{y}) \frac{\partial \tilde{x}}{\partial x}(x) \frac{\partial \tilde{y}}{\partial y}(y)$ , and by

$$\tilde{F}(x, y, s) = \frac{\tilde{u}(x) - \tilde{u}(y)}{w(x - y)} w(s) \tilde{\gamma} \left( \frac{x + y}{2} + \frac{s}{2}, \frac{x + y}{2} - \frac{s}{2} \right)$$

where  $w(s) = \frac{|s|_2^2}{|s|_1}$ . We expand  $\tilde{F}(x, y, s)$  in test functions with respect to  $y$

$$\tilde{F}_h(x, y, s) = \sum_{\mathbf{m}} \tilde{F}(x, x_{\mathbf{m}}, s) \phi_{\mathbf{m}}(y),$$

where  $\phi_{\mathbf{m}}$  is the piecewise bilinear basis function satisfying  $\phi_{\mathbf{m}}(x_{\mathbf{n}}) = 0$  when  $\mathbf{m} \neq \mathbf{n}$  and  $\phi_{\mathbf{m}}(x_{\mathbf{m}}) = 1$ , and give the discrete formulation of  $\tilde{\mathcal{L}}$  by

$$\tilde{\mathcal{L}}_h \hat{u}(x_{\mathbf{n}}) = \sum_{\mathbf{m} \neq \mathbf{n}} \tilde{a}_{\mathbf{n}, \mathbf{m}} \hat{u}(x_{\mathbf{m}}),$$

where

$$\tilde{a}_{\mathbf{n}, \mathbf{m}} = \begin{cases} -\frac{1}{w(x_{\mathbf{m}} - x_{\mathbf{n}})} \int_{\mathbb{R}^2} \left[ \phi_{\mathbf{m}}(y) w(y - x_{\mathbf{n}}) \tilde{\gamma} \left( \frac{x_{\mathbf{m}} + y}{2}, x_{\mathbf{n}} + \frac{x_{\mathbf{m}} - y}{2} \right) \right] dy, & \mathbf{m} \neq \mathbf{n}, \\ -\sum_{\mathbf{m} \neq \mathbf{n}} \tilde{a}_{\mathbf{n}, \mathbf{m}} & \mathbf{m} = \mathbf{n}. \end{cases}$$

We also denote by  $\mathcal{N}$  the set of all nodes in  $\Omega$ , by  $\mathcal{N}_p$  the set of nodes in the PML layer  $\Omega_p$  and by  $\mathcal{N}_b$  the set of nodes in the boundary layer  $\Omega_b$  (Figures 4.1b and 4.1c). The discrete scheme is: finding  $\{\hat{u}_h(x_{\mathbf{n}})\}$  such that

$$\begin{aligned}\tilde{\mathcal{L}}_h \hat{u}_h(x_{\mathbf{n}}) - k^2 \frac{\partial \tilde{x}}{\partial x}(x_{\mathbf{n}}) \hat{u}_h(x_{\mathbf{n}}) &= f(x_{\mathbf{n}}), & x_{\mathbf{n}} \in \mathcal{N} \cup \mathcal{N}_p, \\ \hat{u}_h(x_{\mathbf{n}}) &= 0, & x_{\mathbf{n}} \in \mathcal{N}_b.\end{aligned}$$

## 5 Numerical Examples

In this section, we present some examples in one and two dimensions to illustrate the effectiveness of the PML technique. In subsection 5.1, we consider one dimensional examples. In 1D, several typical kernels are considered and “numerical reflections” generated by large PML coefficient  $z$  are studied. In subsection 5.2, we give several examples with different kernels in two dimensions.

In the following examples, we simply consider the errors between  $u$  and  $\hat{u}_h$  in  $L^2$  norm over  $\Omega$ , i.e.,  $\|u - \hat{u}_h\|_{L^2(\Omega)}$ , where  $u$  represents the “exact” solution. The exact solution for the kernel  $\gamma_r(x - y) = \frac{1}{2c_\gamma^3} e^{-\frac{|x-y|}{c_\gamma}}$  in 1D can be obtained by (3.6), and thus is used to study “numerical reflections” for different PML coefficients  $z$ . The exact solutions for other kernels are obtained by the quadrature-based finite difference discretization on a sufficiently fine mesh of a large domain with sufficiently large  $d_{pml}$ .

### 5.1 One dimension

We first present some examples in one dimension. In this subsection, the absorption coefficient is chosen as

$$\sigma(t) = \begin{cases} 0, & |t| < l, \\ \frac{1}{d_{pml}}(|t| - l), & l \leq |t|. \end{cases}$$

The reader is referred to [16] for more numerical examples for kernels  $\gamma(x, y) = \frac{1}{2c_\gamma^3} e^{-\frac{|x-y|}{c_\gamma}}$  and  $\gamma(x, y) = \frac{4}{\sqrt{\pi}c_\gamma^3} e^{-\frac{(x-y)^2}{c_\gamma^2}}$ , where truncation errors of the PML in both  $L^2$  and  $H^1$  norms as well as the convergence rate of the discrete scheme were considered for imaginary  $z$  or  $z = 0$ .

**Example 1.1:** we first consider the Gaussian kernel  $\gamma(x, y) = \frac{1}{\delta^3} \gamma_0(\frac{|x-y|}{\delta})$  where  $\gamma_0(s) = \frac{1}{2c_0^3} e^{-\frac{|s|}{c_0}}$  and  $c_0$  is a constant such that  $\gamma(1) = 10^{-16}$ . The source is chosen as the Gaussian function  $f(x) = \frac{k}{\sqrt{\pi}} e^{-k^2 x^2}$  and we set  $l = d_{pml} = 1$ .

Figure 5.1 plots the solutions for  $k = 2\pi$  and different  $\delta$ . The numerical solutions are obtained on the mesh with  $h = 1/2^{10}$  and the PML coefficient is  $z = 40(1 + 1i)$ . We remark that the exact solutions are obtained by using (3.6). In subfigure 5.1a, it can be observed that comparing with the exact solution without any modification, the numerical solution for  $k = 2\pi$  and  $\delta = 0.9/(kc_0)$  decays exponentially in PML layers. For  $k = 2\pi$  and  $\delta = 1.1/(kc_0)$ , since the exact solution  $u$  itself decays outside the support of  $f(x)$ , we observe in subfigure 5.1b that the real part of  $\hat{u}_h$  is the same as that of  $u$ , but the PML does come at a price which makes the imaginary part oscillate with an amplitude of 1e-8 in  $\Omega$ .

We study the numerical reflections by this example. To investigate the influence of  $z$  on numerical PML solutions, we present the errors on meshes with  $h = 1/2^n$ , ( $n = 4, 5, \dots, 8$ ) for  $k = 2\pi$  and

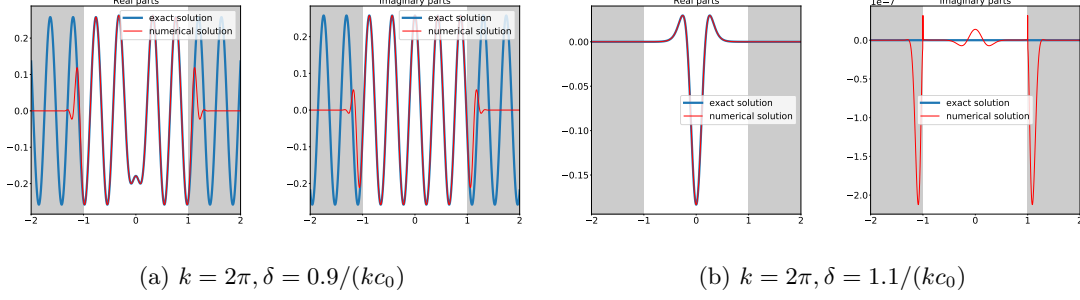


Figure 5.1: Example 1.1: the exact solution  $u$  without any modification and numerical solution  $\hat{u}_h$  for  $k = 2\pi$ ,  $\delta = 0.9/(k\delta_0)$  and  $k = 2\pi$ ,  $\delta = 1.1/(k\delta_0)$ , respectively.  $\hat{u}_h$  is obtained on the mesh with  $h = 1/2^{10}$ . The PML region for numerical solutions are shaded in light grey.

$z = 10i, 20i, 40i, 80i, 160i, 10(1+i), 20(1+i), 40(1+i), 80(1+i), 40(2+i), 40(4+i)$ . Bar graphs in Figure 5.2 show the errors for  $\delta = 0.9/(kc_0)$  where the corresponding exact solution is referred to subfigure 5.1a. It can be seen that vary large  $z$  causes “numerical reflections”. For  $\delta = 1.1/(kc_0)$ , we also compute the errors for  $z = 0$  besides those shown above since the exact solution itself decay exponentially (Theorem [16, Theorem 3] and subfigure 5.1b), which are shown in Figure 5.3. Different from those for  $\delta = 0.9/(kc_0)$ , large  $z$  cause few “numerical reflections”. This result is quite useful in practical usage where there may be no need to consider whether  $\tilde{k}$  is real or complex.

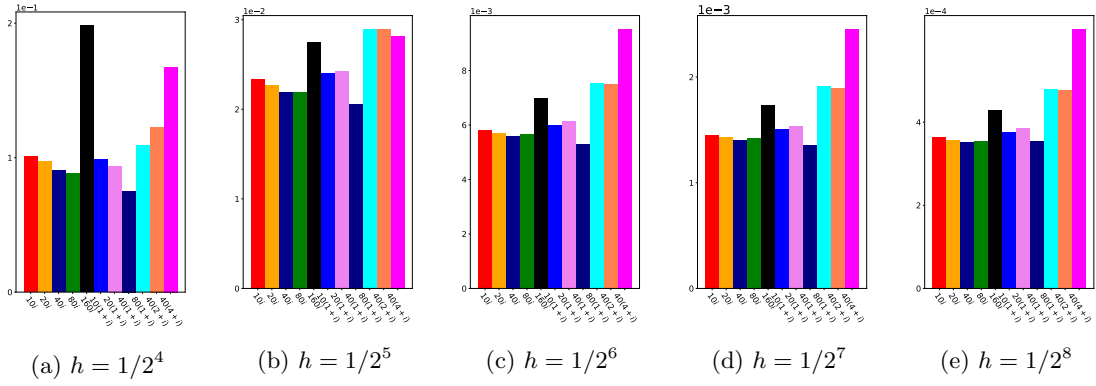


Figure 5.2: Example 1.1: errors for  $k = 2\pi$ ,  $\delta = 0.9/(kc_0)$  and different PML coefficients  $z = 10i, 20i, 40i, 80i, 160i, 10(1+i), 20(1+i), 40(1+i), 80(1+i), 40(2+i), 40(4+i)$ .

Finally, we show the errors for different  $k$  and  $\delta$  in Table 5.1 and the convergence rate of 2 degree for the numerical scheme can be observed, where the PML coefficient is  $z = 40(1+i)$ .

**Example 1.2:** Here we consider the fractional Helmholtz equation

$$(-\Delta)^s u(x) - k^2 u(x) = f(x), \quad (0 < s < 1)$$

where

$$(-\Delta)^s = C(s) \text{ p.v. } \int_{\mathbb{R}} \frac{u(x) - u(y)}{|x - y|^{1+2s}} dy, \quad C(s) = \frac{2^{2s} s \Gamma(s + \frac{1}{2})}{\pi^{\frac{1}{2}} \Gamma(1 - s)}.$$

Note that this kernel  $\gamma = C(s)/|x - y|^{1+2s}$  is nonintegrable.

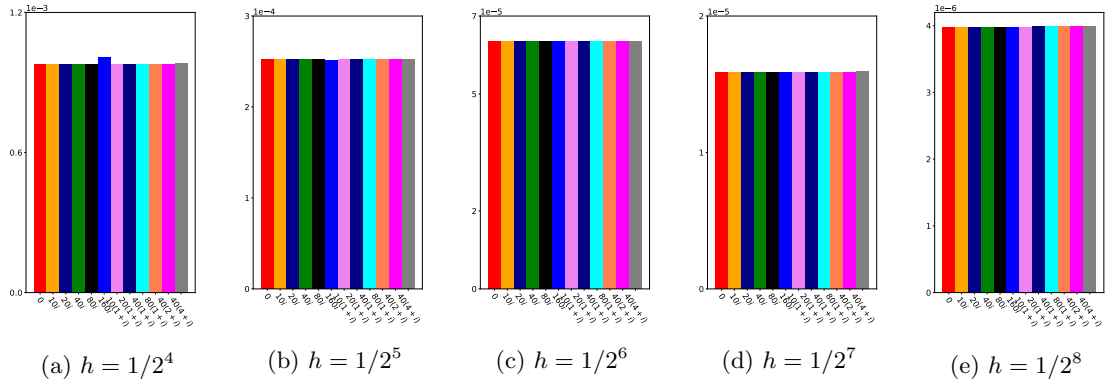


Figure 5.3: Example 1.1: errors for  $k = 2\pi$ ,  $\delta = 1.1/(k\delta_0)$  and different PML coefficients  $z = 0, 10i, 20i, 40i, 80i, 160i, 10(1+i), 20(1+i), 40(1+i), 80(1+i), 40(2+i), 40(4+i)$ .

		$\delta = 0.9/(k\delta_0)$		$\delta = 1.1/(k\delta_0)$	
		$2\pi$	$4\pi$	$2\pi$	$4\pi$
$h$	$k$				
$1/2^3$		2.6916e-01	9.3425e-02	3.6272e-03	5.5867e-03
$1/2^4$		7.5197e-02	2.1346e-01	9.7979e-04	1.2606e-03
$1/2^5$		2.0569e-02	8.1455e-02	2.5213e-04	3.4335e-04
$1/2^6$		5.2943e-03	2.0284e-02	6.3396e-05	8.8716e-05
$1/2^7$		1.3574e-03	4.9203e-03	1.5857e-05	2.2355e-05
$1/2^8$		3.5401e-04	1.2200e-03	3.9626e-06	5.6008e-06

Table 5.1: Example 1.1:  $L^2$  errors of numerical solutions with the PML coefficient  $z = 40(1+i)$ .

The source function is still the Gaussian function  $f(x) = \frac{k}{\sqrt{\pi}}e^{-k^2x^2}$ , and we set  $l = d_{pml} = 10$ .

Figure 5.4 plots the reference solutions and numerical solutions for  $s = 1/2$  and  $k = 2\pi/10, 32\pi/10$ , respectively. The reference solutions are obtained by the quadrature-based finite difference discretization over a large domain with sufficiently large  $d_{pml}$ . The numerical solutions are obtained on the mesh with  $h = 1/2^{10}$  and the PML coefficient  $z$  is set to be  $10(15 + i)$ . It can be observed that the real part to  $z$  makes the wave oscillate faster in the PML region, which possibly comes at a price, that is exacerbating the numerical reflections.

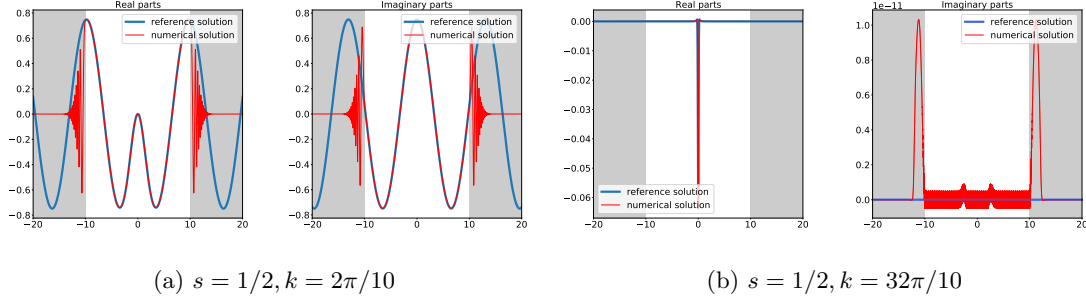


Figure 5.4: Example 1.2: the reference solution and numerical solution  $\hat{u}_h$  for  $s = 1/2$  and  $k = 2\pi/10, 32\pi/10$ , respectively.  $\hat{u}_h$  is obtained on the mesh with  $h = 1/2^{10}$ . The PML region for numerical solutions are shaded in light grey.

We also list the errors for  $s = 1/4, 1/2, 3/4$  and different  $k$  in Table 5.2.

s \ k	1/4		1/2		3/4
	2π/10	32π/10	2π/10	32π/10	2π/10
1/2 <sup>3</sup>	6.4579e-01	1.8313e-04	2.5225e-00	6.2172e-04	5.7245e-01
1/2 <sup>4</sup>	5.1598e-01	8.7411e-05	1.5536e-00	3.6704e-04	7.8702e-01
1/2 <sup>5</sup>	2.1102e-01	2.5361e-05	1.6200e-01	1.6050e-04	1.9043e-01
1/2 <sup>6</sup>	5.3547e-03	4.5099e-06	1.3190e-02	4.9687e-05	6.3030e-03
1/2 <sup>7</sup>	1.3582e-03	9.7128e-07	3.2176e-03	9.2833e-06	1.1760e-03
1/2 <sup>8</sup>	2.8050e-04	1.8949e-07	8.6243e-04	2.0942e-06	2.3323e-04

Table 5.2: Example 1.2:  $L^2$  errors for  $s = 1/4, 1/2, 3/4$  and different  $k$ .

**Example 1.3:** here we take a discontinuous kernel  $\gamma(x, y) = \frac{3}{\delta^3}\chi_{[-\delta, \delta]}(|x - y|)$ . The source function is still  $f(x) = \frac{k}{\sqrt{\pi}}e^{-k^2x^2}$ , and we set  $l = d_{pml} = 1$ .

Since this kernel is discontinuous at points  $|x - y| = \delta$ , a new difficulty is to analytically continue the kernel into complex plane. We first approximate  $\chi_{[-1, 1]}(s)$  by a smooth function

$$\hat{\chi}_{[-1, 1]}(s) = \frac{1}{2} \left( \frac{e^{-\tau(|s|-1)} - 1}{e^{-\tau(|s|-1)} + 1} + 1 \right), \text{ where } \tau = -\frac{\ln tol}{\epsilon_0}. \quad (5.1)$$

It's clear that  $\hat{\chi}_{[-1, 1]}(s)$  converges to  $\chi_{[-1, 1]}(s)$  as  $tol$  and  $\epsilon_0$  go to zero (Figure 5.5). In practical computation, we replace the kernel  $\gamma(x, y) = \frac{3}{\delta^3}\chi_{[-\delta, \delta]}(|x - y|)$  by

$$\hat{\gamma}(x, y) = \frac{3}{\delta^3} \hat{\chi}_{[-1, 1]} \left( \frac{|x - y|}{\delta} \right)$$

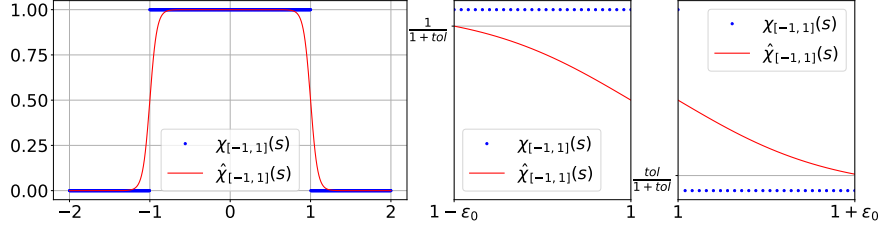


Figure 5.5: Example 1.4:  $\chi_{[-1,1]}(s)$  and  $\hat{\chi}_{[-1,1]}(s)$ .

where  $tol = \epsilon_0 = 0.01$ .

Figure 5.6 plots the solutions for  $\delta = 1/4$  and  $k = 2\pi, 4\pi$ , respectively. The PML coefficient  $z$  is equal to  $40(10 + i)$ . It can be observed that the solutions decay exponentially outside  $\Omega$  and the real part to  $z$  make the wave oscillate faster in the PML region.

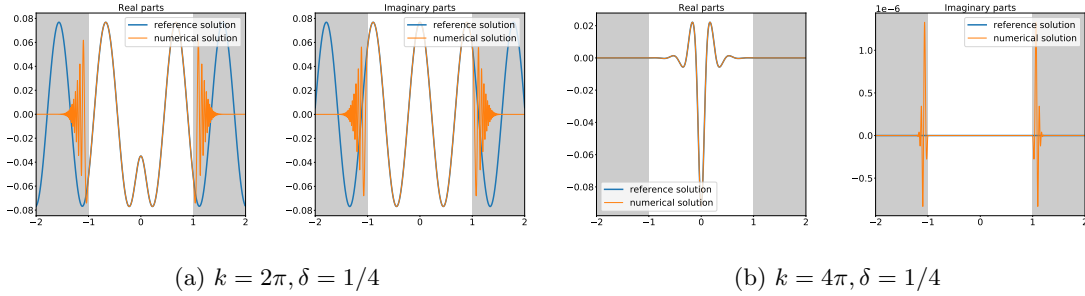


Figure 5.6: Example 1.3: the reference solution and numerical solution  $\hat{u}_h$  for  $\delta = 1/4$  and  $k = 2\pi, 4\pi$ , respectively.  $\hat{u}_h$  is obtained on the mesh with  $D_f = 2^{12} - 1$ . The PML region for numerical solutions are shaded in light grey.

Table 5.3 shows the errors for  $\delta = 1/4$  and different  $k$ .

$h \backslash k$	$2\pi$	$4\pi$
$1/2^3$	6.4581e-02	2.6907e-03
$1/2^4$	2.2103e-01	8.9758e-04
$1/2^5$	5.0557e-02	2.3435e-04
$1/2^6$	6.4625e-03	5.9073e-05
$1/2^7$	2.5531e-04	1.4621e-05
$1/2^8$	7.7875e-05	3.4811e-06

Table 5.3: Example 1.3:  $L^2$  errors for  $\delta = 0.25$ .

## 5.2 Two dimensions

Here we consider three examples in two dimensions. For PMLs in Cartesian coordinates, we choose  $\Omega = [-l, l]^2$  and  $\Omega_p = \Omega_p^s$  (4.1), and set

$$\sigma_1(t) = \sigma_2(t) = \begin{cases} 0, & -l \leq t \leq l, \\ \frac{1}{d_{pml}}(|t| - l), & l < |t|. \end{cases} \quad (5.2)$$

For PMLs in polar coordinates, we choose  $\Omega = \{x \in \mathbb{R}^2 : |x|_2 \leq l_r\}$  and  $\Omega_p = \Omega_p^c$  (4.2) and set

$$\sigma_r(t) = \begin{cases} 0, & 0 \leq t \leq l_r, \\ \frac{1}{d_{pml}}(t - l_r), & l_r < t. \end{cases} \quad (5.3)$$

Figure 5.7 illustrates meshes used in the following examples for PMLs in Cartesian coordinates and polar coordinates, respectively.

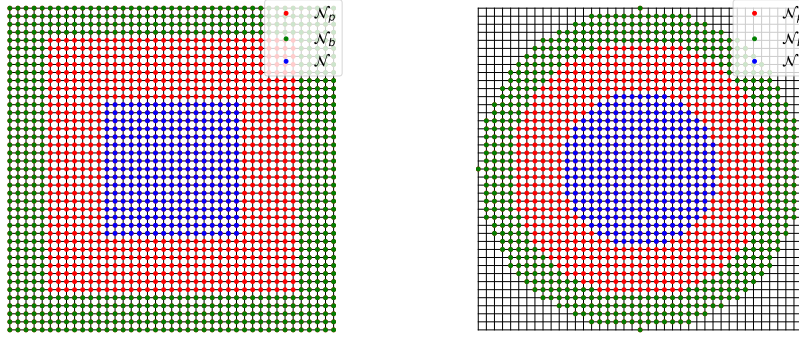


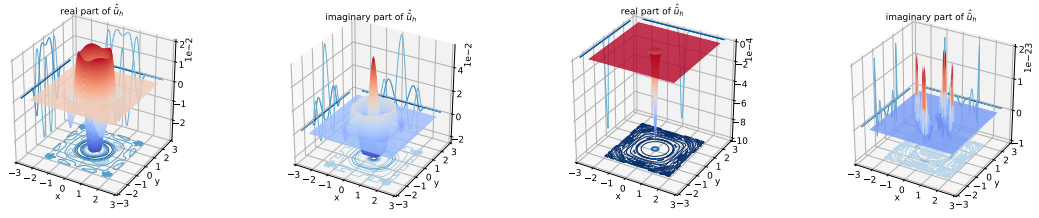
Figure 5.7: Two dimensional meshes for PMLs in Cartesian coordinates (left) and polar coordinates (right).

**Example 2.1:** we first consider the exponential kernel  $\gamma(x, y) = \frac{1}{\delta^4} \gamma_0(\frac{|x-y|}{\delta})$ ,  $(x, y \in \mathbb{R}^2)$ , where  $\gamma_0(s) = \frac{1}{3\pi c_0^4} e^{-\frac{|s|}{c_0}}$  and  $c_0$  is such that  $\gamma_0(1) = 10^{-10}$ . The source function is  $f(x) = 2\sqrt{\pi} e^{-4\pi^2|x|^2}$ . We set the PML coefficient  $z = 40i$  and set  $l_r = l = d_{pml} = 1$ .

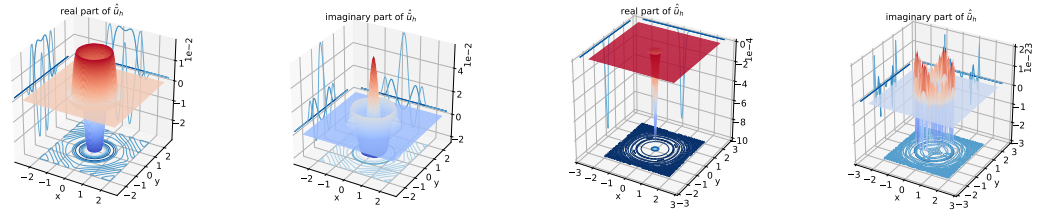
We plot some numerical solutions and projections of their contours on the ‘walls’ of graphs for each dimension in Figure 5.8. We can observe that behaviors of the solutions is similar to those in one dimension in some sense. For  $k = 2\pi$  and  $\delta = 0.1/(kc_0)$ , numerical solutions by PMLs in both Cartesian coordinates and polar coordinates oscillate in  $\Omega$  and decay exponentially outside  $\Omega$ . For  $k = 20\pi$  and  $\delta = 1/(kc_0)$ , the solutions themselves decay outside the support of  $f(x)$ , but PMLs make their imaginary parts oscillate at a amplitude of  $2e-23$  in  $\Omega$ .

Table 5.4 shows the errors for  $k = 2\pi, \delta = 0.1/(kc_0)$  and  $k = 20\pi, \delta = 1/(kc_0)$ . We observe that the convergence rates for  $k = 2\pi$  and  $\delta = 0.1/(kc_0)$  are less than 2, which is possibly due to the error not being in the asymptotic regime.

**Example 2.2:** here we consider the Gaussian kernel  $\gamma(x, y) = \frac{1}{\delta^4} \gamma_0(\frac{|x-y|}{\delta})$ ,  $(x, y \in \mathbb{R}^2)$ , where  $\gamma_0(s) = \frac{4}{\pi c_0^4} e^{-\frac{s^2}{c_0^2}}$  and  $c_0$  is set such that  $\gamma_0(1) = 10^{-10}$ . The source function is still  $f(x) = 2\sqrt{\pi} e^{-4\pi^2|x|^2}$ . The PML coefficient is  $z = 40(2 + i)$  and we set  $l_r = l = d_{pml} = 1$ .



(a)  $k = 2\pi, \delta = 0.1/(kc_0)$  by PMLs in Cartesian coordinates (b)  $k = 20\pi, \delta = 1/(kc_0)$  by PMLs in Cartesian coordinates



(c)  $k = 2\pi, \delta = 0.1/(kc_0)$  by PMLs in polar coordinates (d)  $k = 20\pi, \delta = 1/(kc_0)$  by PMLs in polar coordinates

Figure 5.8: Example 2.1: numerical solutions  $\hat{u}_h$  for the exponential kernel by PMLs in Cartesian coordinates and polar coordinates.

		$k = 2\pi, \delta = 0.1/(kc_0)$		$k = 20\pi, \delta = 1/(kc_0)$	
$h$	PML	CPML	PPML	CPML	PPML
		1/2	7.2967e-02	3.2462e-02	1.0402e-05
	1/2 <sup>2</sup>	4.6085e-02	1.4093e-02	3.1928e-06	1.4900e-06
	1/2 <sup>3</sup>	3.2165e-03	2.1774e-03	6.2513e-07	3.0248e-07
	1/2 <sup>4</sup>	9.6998e-04	8.8405e-04	1.0088e-07	4.9637e-08

Table 5.4: Example 2.1:  $L^2$  errors for the exponential kernel by PMLs. CPML and PPML are short for PMLs in Cartesian coordinates and polar coordinates, respectively.

Figure 5.9 plots the numerical solutions for  $k = 2\pi, \delta = 0.6/(kc_0)$  and  $k = 20\pi, \delta = 6/(kc_0)$  by two kinds of PMLs. We observe that the solution for  $k = 2\pi, \delta = 0.6/(kc_0)$  decays exponentially in the absorbing layers, and the solution for  $k = 20\pi, \delta = 6/(kc_0)$  itself decays exponentially outside the support of  $f$  where the oscillation of its imaginary part at an amplitude of  $8e-19$  may be a result of numerical reflections by PMLs.

Table 5.5 shows the errors on meshes with different mesh size  $h$ .

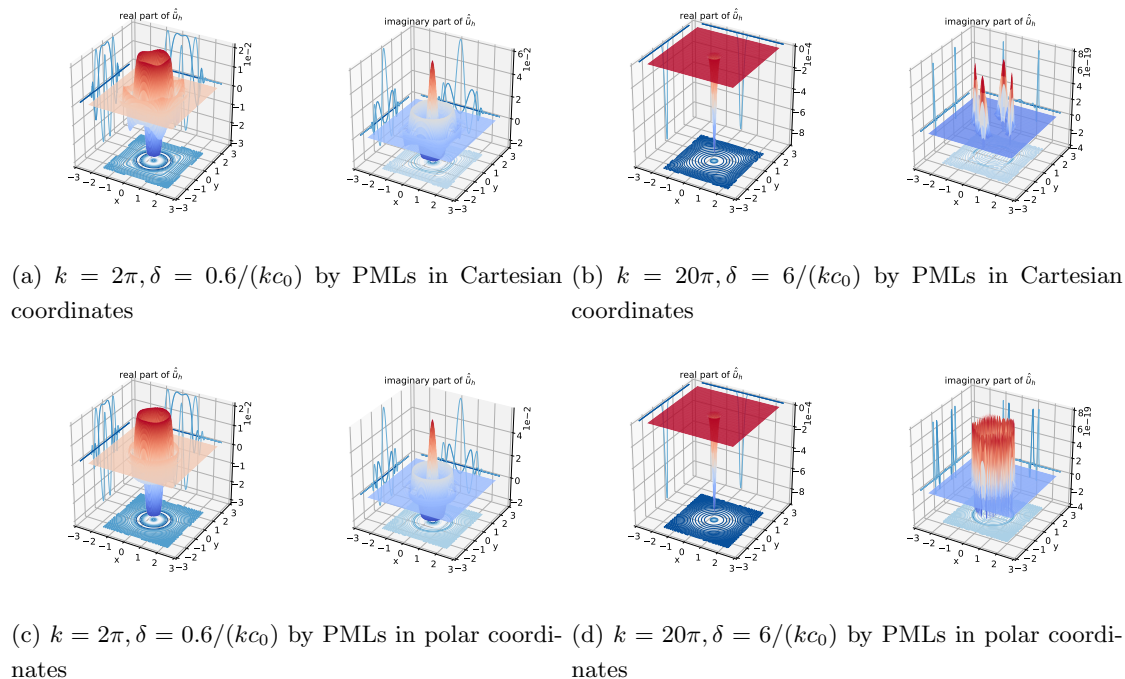


Figure 5.9: Example 2.2: numerical solutions  $\hat{u}_h$  for the Gaussian kernel by PMLs in Cartesian coordinates and polar coordinates.

		$k = 2\pi, \delta = 0.6/(kc_0)$		$k = 20\pi, \delta = 6/(kc_0)$	
PML		CPML	PPML	CPML	PPML
$h$					
	1/2	7.0802e-02	3.1428e-02	8.0159e-06	3.4354e-06
	1/2 <sup>2</sup>	2.6993e-01	2.3136e-02	2.2633e-06	1.0562e-06
	1/2 <sup>3</sup>	6.4693e-03	3.2647e-03	3.1686e-07	1.5332e-07
	1/2 <sup>4</sup>	1.7444e-03	1.2298e-03	5.7803e-08	2.8443e-08

Table 5.5: Example 2.2:  $L^2$  errors of solutions for the Gaussian kernel by PMLs. CPML and PPML are short for PMLs in Cartesian coordinates and polar coordinates, respectively.

**Example 2.3:** we also consider the piecewise constant kernel  $\gamma(x, y) = \frac{8}{\pi\delta^4} \chi_{[-\delta, \delta]}(|x-y|)$ , ( $x, y \in \mathbb{R}^2$ ). To analytically continue this discontinuous kernel into complex plane, we first approximate it by the smooth function (5.1), which is the kernel used in the following computation.

The source function is taken as  $f(x) = 2\sqrt{\pi}e^{-4\pi^2|x|^2}$ . The PML coefficient is  $z = 40(2 + i)$  and we set  $l_r = l = d_{pml} = 1$ .

Figure 5.10 plots the numerical solutions for  $k = 2\pi, \delta = 0.5$  and  $k = 20\pi, \delta = 0.5$  by two kinds of PMLs. Table 5.6 shows the errors for different  $h$  and  $k$ . We observe that in this example, PMLs in polar coordinates perform better than PMLs in Cartesian coordinates.

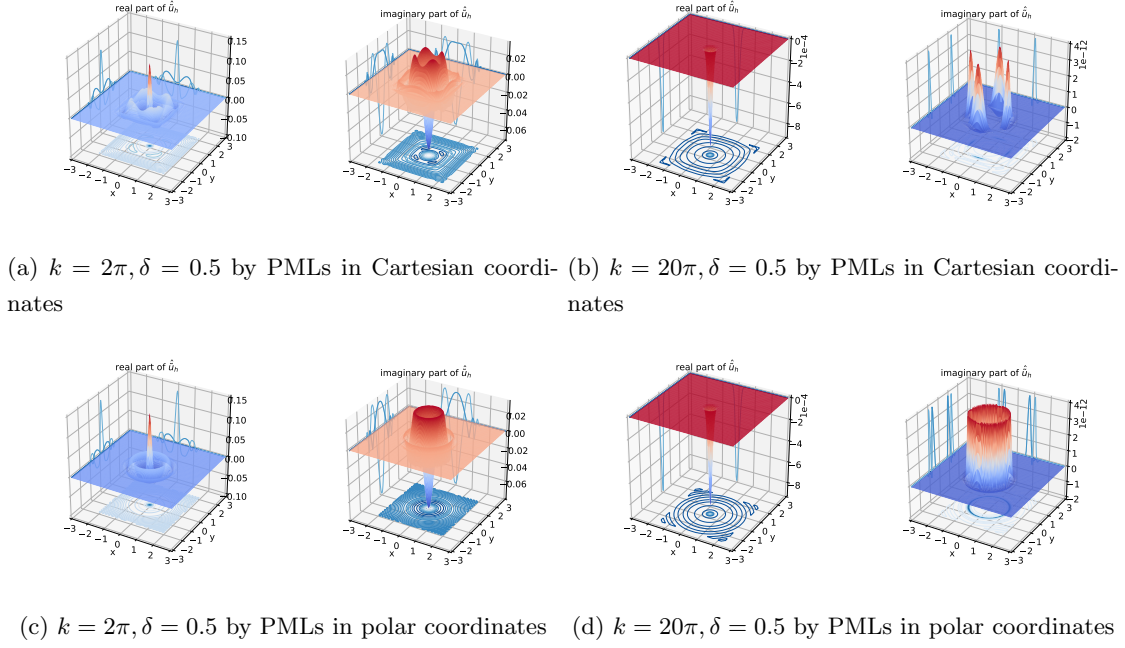


Figure 5.10: Example 2.3: numerical solutions  $\hat{u}_h$  for the piecewise constant kernel by PMLs in Cartesian coordinates and polar coordinates.

PML		$k = 2\pi, \delta = 0.5$		$k = 20\pi, \delta = 0.5$	
		CPML	PPML	CPML	PPML
$h$	$1/2$	1.7371e-01	7.8477e-02	2.3698e-06	1.0156e-06
	$1/2^2$	1.9225e-02	1.3591e-02	2.1050e-07	9.8233e-08
	$1/2^3$	5.9661e-03	2.8118e-03	3.6687e-08	1.7752e-08
	$1/2^4$	3.4068e-03	7.7588e-04	7.1255e-09	3.5062e-09

Table 5.6: Example 2.3:  $L^2$  errors of solutions for the piecewise constant kernel for PMLs. CPML and PPML are short for PMLs in Cartesian coordinates and polar coordinates, respectively.

**Example 2.4:** we finally consider the fractional Helmholtz equation in 2D

$$(-\Delta)^s u(x) - k^2 u(x) = f(x), \quad x \in \mathbb{R}^2, \quad (0 < s < 1) \quad (5.4)$$

where

$$(-\Delta)^s u(x) = C(2, s) \text{ p.v. } \int_{\mathbb{R}^2} \frac{u(x) - u(y)}{|x - y|^{2+2s}} dy, \quad C(2, s) = \frac{2^{2s} s \Gamma(s + 1)}{\pi \Gamma(1 - s)}.$$

We choose the source function  $f(x) = \frac{\sqrt{\pi}}{5} e^{-\frac{\pi^2}{25}|x|^2}$ , and set  $z = 40(2 + i)$  and  $l_r = l = d_{pml} = 10$ .

We here solve PML problems for  $s = 1/2$  and  $k = \frac{\pi}{5}, \frac{16\pi}{5}$ . The corresponding solutions are plotted in Figure 5.11 and the errors are shown in Table 5.7. The behaviors of solutions are quite similar to those examples above.

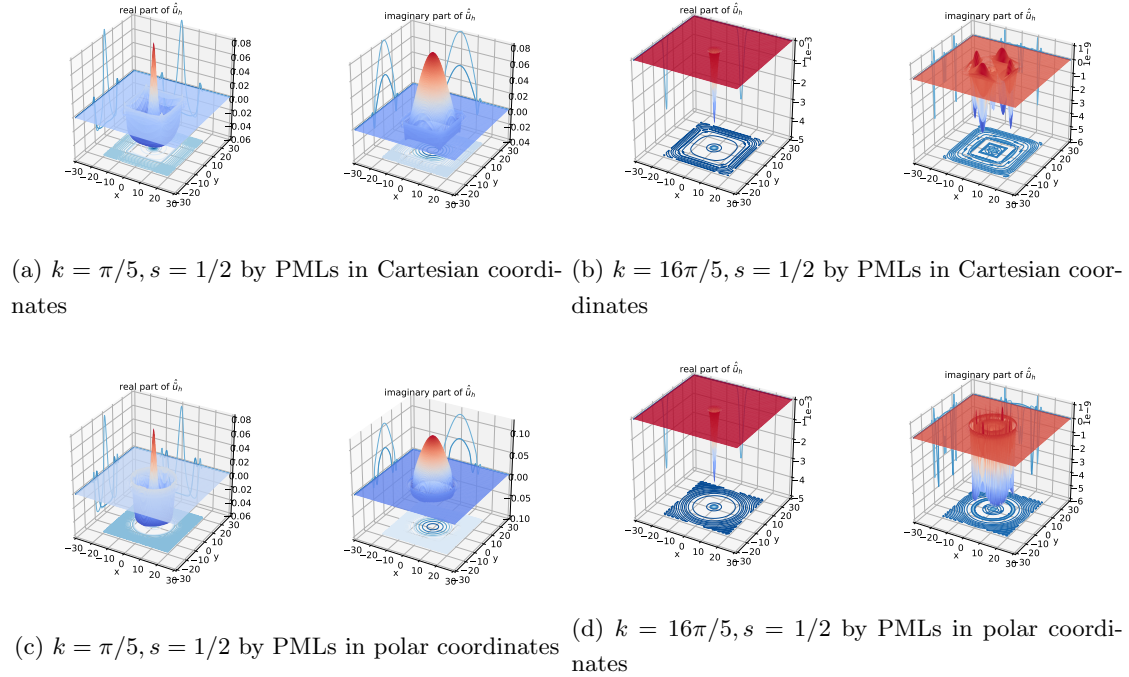


Figure 5.11: Example 2.4: numerical solutions  $\hat{u}_h$  of fractional Helmholtz equations by PMLs in Cartesian coordinates and polar coordinates.

PML		$k = \pi/5, s = 0.5$		$k = 16\pi/5, s = 0.5$	
		CPML	PPML	CPML	PPML
$h(*10)$					
	1/2	1.5120e-01	5.0111e-01	4.4503e-05	1.9081e-05
	1/2 <sup>2</sup>	6.7320e-02	1.1692e-01	1.1025e-05	5.1440e-06
	1/2 <sup>3</sup>	1.1717e-01	8.7647e-02	1.8385e-06	8.8968e-07
	1/2 <sup>4</sup>	1.6673e-02	1.9219e-02	3.5580e-07	1.7510e-07

Table 5.7: Example 2.4:  $L^2$  errors of solutions of fractional Helmholtz equations by PMLs. CPML and PPML are short for PMLs in Cartesian coordinates and polar coordinates, respectively.

## References

- [1] B. ALPERT, L. GREENGARD, AND T. HAGSTROM, *Rapid evaluation of nonreflecting boundary kernels for time-domain wave propagation*, SIAM J. Numer. Anal., 37 (2000), pp. 1138–1164.
- [2] X. ANTOINE AND E. LORIN, *Towards perfectly matched layers for time-dependent space fractional pdes*, Journal of Computational Physics, 391 (2019), pp. 59–90.

- [3] A. ARNOLD, M. EHRHARDT, AND I. SOFRONOV, *Approximation and fast calculation of non-local boundary conditions for the time-dependent Schrödinger equation*, Domain Decomposition Methods in Science and Engineering. Springer, Berlin, Heidelberg, (2005), pp. 141–148.
- [4] G. BAO AND H. WU, *Convergence analysis of the PML problems for time-harmonic Maxwell's equations*, SIAM J. Numer. Anal., 43 (2005), pp. 2121–2143.
- [5] J.-P. BÉRENGER, *A perfectly matched layer for the absorption of electromagnetic waves*, J. Comput. Phys., 114 (1994), pp. 185–200.
- [6] ———, *Three-dimensional perfectly matched layer for the absorption of electromagnetic waves*, J. Comput. Phys., 127 (1996), pp. 363–379.
- [7] J. H. BRAMBLE AND J. E. PASCIAK, *Analysis of a finite PML approximation for the three dimensional time-harmonic maxwell and acoustic scattering problems*, Math. Comput., 76 (2006), pp. 597–614.
- [8] W. CHEN AND W. WEEDOM, *A 3d perfectly matched medium from modified Maxwell's equations with stretched coordinates*, Microwave Opt. Tech. Lett., 7 (1994), pp. 599–604.
- [9] X. CHEN AND M. GUNZBURGER, *Continuous and discontinuous finite element methods for a peridynamics model of mechanics*, Computer Methods in Applied Mechanics and Engineering, 200 (2011), pp. 1237–1250.
- [10] Z. CHEN AND X. LIU, *An adaptive perfectly matched layer technique for time-harmonic scattering problems*, SIAM J. Numer. Anal., 43 (2005), pp. 645–671.
- [11] Z. CHEN AND H. WU, *An adaptive finite element method with perfectly matched absorbing layers for the wave scattering by periodic structures*, SIAM J. Numer. Anal., 41 (2003), pp. 799–826.
- [12] F. COLLINO AND P. MONK, *The perfectly matched layer in curvilinear coordinates*, SIAM J. Sci. Comput., 19 (1998), pp. 2061–2090.
- [13] Q. DU, M. GUNZBURGER, R. B. LEHOUCQ, AND K. ZHOU, *Analysis and approximation of nonlocal diffusion problems with volume constraints*, SIAM Rev., 54 (2012), pp. 667–696.
- [14] Q. DU, M. D. GUNZBURGER, R. B. LEHOUCQ, AND K. ZHOU, *Analysis and approximation of nonlocal diffusion problems with volume constraints*, Siam Rev., 54 (2012), pp. 667–696.
- [15] Q. DU, J. ZHANG, AND C. ZHENG, *Nonlocal wave propagation in unbounded multi-scale media*, Commun. Comput. Phys., 24 (2018).
- [16] Y. DU AND J. ZHANG, *Numerical solution of a one-dimensional nonlocal Helmholtz equation by perfectly matched layers*, arXiv preprint arXiv:2007.11193, (2020).
- [17] E. EMMRICH AND O. WECKNER, *Analysis and numerical approximation of an integro-differential equation modeling non-local effects in linear elasticity*, Mathematics and Mechanics of Solids, 12 (2007), pp. 363–384.
- [18] M. J. GROTE AND J. B. KELLER, *Exact nonreflecting boundary conditions for the time dependent wave equation*, SIAM J. Appl. Math., 55 (1995), pp. 280–297.

- [19] T. HAGSTROM, A. MAROR, AND D. GIVOLI, *High-order local absorbing conditions for the wave equation: Extensions and improvements*, J. Comput. Phys., 227 (2008), pp. 3322–3357.
- [20] H. HAN AND Z. HUANG, *A class of artificial boundary conditions for heat equation in unbounded domains*, Comput. Math. Appl., 43 (2002), pp. 889–900.
- [21] H. HAN AND C. ZHENG, *Exact nonreflecting boundary conditions for an acoustic problem in three dimensions*, J. Comput. Math., 21 (2003), pp. 15–24.
- [22] T. HOHAGE, F. SCHMIDT, AND L. ZSCHIEDRICH, *Solving time-harmonic scattering problems based on the pole condition II: Convergence of the pml method*, SIAM J. Math. Anal., 35 (2003), pp. 547–560.
- [23] M. LASSAS AND E. SOMERSALO, *On the existence and convergence of the solution of PML equations*, Computing, 60 (1998), pp. 229–241.
- [24] Y. LI AND H. WU, *FEM and CIP-FEM for Helmholtz equation with high wave number and Perfectly Matched Layer truncation*, SIAM J. Numer. Anal., 57 (2019), pp. 96–126.
- [25] R. W. MACEK AND S. A. SILLING, *Peridynamics via finite element analysis*, Finite Elements in Analysis and Design, 43 (2007), pp. 1169–1178.
- [26] J. M. MELENK AND S. SAUTER, *Convergence analysis for finite element discretizations of the Helmholtz equation with Dirichlet-to-Neumann boundary conditions*, Math. Comp., 79 (2010), pp. 1871–1914.
- [27] J. Z. Q. DU, H. HAN AND C. ZHENG, *Numerical solution of a two-dimensional nonlocal wave equation on unbounded domains*, SIAM J. Sci. Comput., 40 (2018), pp. 1430–1445.
- [28] Y. TAO, X. TIAN, AND Q. DU, *Nonlocal diffusion and peridynamic models with Neumann type constraints and their numerical approximations*, Appl. Math. Comput., 305, pp. 282–298.
- [29] Z. TENG, *Exact boundary condition for time-dependent wave equation based on boundary integral*, J. Comput. Phys., 190 (2003), pp. 398–418.
- [30] X. TIAN AND Q. DU, *Analysis and comparison of different approximations to nonlocal diffusion and linear peridynamic equations*, SIAM J. Numer. Anal., 51 (2013), pp. 3458–3482.
- [31] ———, *Asymptotically compatible schemes and applications to robust discretization of nonlocal models*, SIAM J. Numer. Anal., 52 (2014), pp. 1641–1665.
- [32] E. TURKEL AND A. YEFET, *Absorbing pml boundary layers for wave-like equations*, Appl. Numer. Math., 27 (1998), pp. 533–557.
- [33] R. A. WILDMAN AND G. A. GAZONAS, *A perfectly matched layer for peridynamics in two dimensions*, J. Mech. Mater. Struct., 7 (2012), pp. 765–781.
- [34] W. ZHANG, J. YANG, J. ZHANG, AND Q. DU, *Absorbing boundary conditions for nonlocal heat equations on unbounded domain*, Commun. Comput. Phys., 21 (2017), pp. 16–39.
- [35] C. ZHENG, J. HU, Q. DU, AND J. ZHANG, *Numerical solution of the nonlocal diffusion equation on the real line*, SIAM J. Sci. Comput., 39 (2017), pp. 1951–1968.
- [36] K. ZHOU AND Q. DU, *Mathematical and numerical analysis of linear peridynamic models with nonlocal boundary conditions*, SIAM J. Numer. Anal., 48 (2010), pp. 1759–1780.